

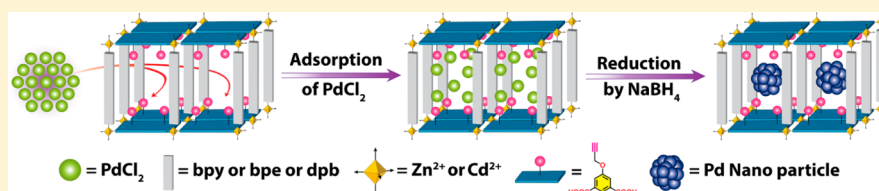
High Loading of Pd Nanoparticles by Interior Functionalization of MOFs for Heterogeneous Catalysis

Bappaditya Gole,[†] Udishnu Sanyal,[†] Rahul Banerjee,[‡] and Partha Sarathi Mukherjee^{*,†}

[†]Department of Inorganic and Physical Chemistry, Indian Institute of Science, Bangalore 560012, India

[‡]Physical and Materials Chemistry Division, CSIR-National Chemical Laboratory, Dr. Homi Bhabha Road, Pune 411008, India

Supporting Information



ABSTRACT: In this report, the issue related to nanoparticle (NP) agglomeration upon increasing their loading amount into metal–organic frameworks (MOFs) has been addressed by functionalization of MOFs with alkyne groups. The alkyneophilicity of the Pd²⁺ (or other noble metals) ions has been utilized successfully for significant loading of Pd NPs into alkyne functionalized MOFs. It has been shown here that the size and loading amount of Pd NPs are highly dependent on the surface area and pore width of the MOFs. The loading amount of Pd NPs was increased monotonically without altering their size distribution on a particular MOF. Importantly, the distinct role of alkyne groups for Pd²⁺ stabilization has also been demonstrated by performing a control experiment considering a MOF without an alkyne moiety. The preparation of NPs involved two distinct steps viz. adsorption of metal ions inside MOFs and reduction of metal ions. Both of these steps were monitored by microscopic techniques. This report also demonstrates the applicability of Pd@MOF NPs as extremely efficient heterogeneous catalysts for Heck-coupling and hydrogenation reactions of aryl bromides or iodides and alkenes, respectively.

INTRODUCTION

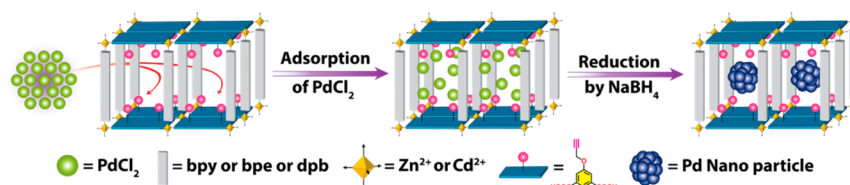
Catalysts are often used to generate energy carriers like hydrogen and hydrocarbon fuels in the chemical industry and also in the conversion of chemical energy from fuel to electricity.¹ The efficiency of metal nanoparticles (MNPs) as heterogeneous catalysts depends on their nanostructure (e.g., size, shape, and crystal orientation) and composition.² Thus, nanoparticles with precisely controlled shapes and sizes are the key requirements to realize the best catalytic activity. Generally, the nanoparticles are prepared by reducing the suitable metal precursor(s) in the presence of a reducing agent wherein the size is primarily achieved by the judicious choice of surfactants which are mostly the organic capping ligands and/or polymers.³ However, from the catalysis perspective the presence of surfactant is detrimental because it blocks the surface site which essentially deactivates the catalyst surface.⁴ Also organic capping agents stabilizing NPs often limit their application in high temperature catalytic reactions. The use of porous materials in this regard is particularly promising because they not only provide the surfactant free specific surface site but also allow nucleation and growth in a confined cavity, thus stabilizing the particles in nanosize regime. Although porous materials such as microporous zeolites, mesoporous silica, and various others inorganic/organic materials have been used,⁵ metal-organic-frameworks (MOFs) or porous co-ordination polymers are emerging as the most promising stabilizing agents from this family owing to their rationally designed framework

structure, tunable pore size of the order of molecular dimension, and chemical tailoring of the inner surface of the channels and cavities.⁶ It has been evident from the precedent literature that the presence of the pore walls helps to prevent the agglomeration of the NPs, thus resulting in narrow particle size and size distribution.

Generally, two major synthetic approaches are used to stabilize MNPs onto the porous architecture of MOFs.⁷ The first and most widely used one is initially the immobilization of a suitable metal precursor inside the cavity of MOFs which subsequently reduced or decomposed to generate metal atoms.⁸ Here, growth of the MNPs is controlled by the pore dimension of the respective MOFs. Various synthetic techniques such as chemical vapor deposition (CVD),⁹ solution infiltration,¹⁰ and solid grinding^{8c,e} are used to immobilize the metal precursor inside the MOFs cavity efficiently. Though all these methodologies are easy to handle, most often the deposition of the particles takes place on the outer surface of MOF structure. The second and most recent approach demonstrated polymer capped MNPs initially synthesized, and then, the MOF structure was allowed to grow around it using the appropriate chemicals.¹¹ However, Xu and co-workers used another method, which is completely different from the previous two approaches, termed as the “double solvent

Received: November 25, 2015

Scheme 1. Schematic Illustration of the Synthesis of Pd NPs Supported by MOFs via the Two-Step Mechanism



approach” to prepare the ultrafine Pt nanoparticles inside the MIL-101 pore.¹²

Although considerable attention has been paid in this direction, a facile methodology is still important to provide the selective immobilization of different metal precursors inside the MOF cavities and control their nucleation and growth. Another important issue which has not been much highlighted in the recent past is the amount of loading of metal nanoparticles without aggregation. Uniform distribution of MNPs with small sizes was realized only for the lower loading amount due to the negligible interaction with metal ions or MNPs and MOFs. Functionalization of MOFs is one promising way which could enhance metal loading by strong electronic interaction with the metal ions.

Herein, we report the functionalization of building ligand with a bare ethynyl moiety and its successful use in the synthesis of MOFs. As anticipated, the single crystal structures of the Zn-MOFs of the corresponding ligand showed that the ethynyl moieties are pointed toward the pore. It is known that the noble metal ions can strongly interact with the ethynyl functionality through its distinct π -donation and π -acceptor characteristics.¹³ This tends to stabilize noble metal ions preferentially and thus can facilitate significantly high metal loading into MOFs (Scheme 1). Because of the presence of alkyne moieties, initially, Au and Pd metal ions were immobilized uniformly throughout the MOF matrix via the solvent impregnation method. Subsequent reduction of those produced MNPs, wherein alkyne group acts as a stabilizer to control the growth of the particles and thus result in narrow-size particles. We have demonstrated earlier the exceptional loading of Au NPs (~ 50 wt %, 1.85 ± 0.3 nm) into MOFs without altering their monodispersity and particle size.¹⁴ Herein, we report a systematic study on the stabilization of Pd NPs in different porous MOFs with interior alkyne functionalization because of the high interest in the chemical industry for heterogeneous catalysts for many organic reactions. It is also demonstrated here that the loading amount can be monitored depending upon the porosity of the MOFs. Finally, the supported Pd NPs were used for heterogeneous Heck-coupling reactions and efficient hydrogenation of alkenes with high reusability.

EXPERIMENTAL SECTION

Synthesis and General Characterizations. MOF-1 [$Zn(pip)(bpy)$], MOF-2(Zn) [$Zn(pip)(bpe)$], and MOF-3 [$Zn(pip)(dpb)$] were synthesized according to our previously published report and characterized thoroughly.¹⁴ The ligands: H_2pip , bpy , bpe , and dpb have their usual names, 5-(prop-2-yn-1-yloxy)isophthalic acid, 4,4'-bipyridine, 1,2-di(pyridin-4-yl)ethane, and 1,4-di(pyridin-4-yl)benzene, respectively.

Synthesis of MOF-2(Cd) [$Cd(pip)(bpe)$]. $Cd(NO_3)_2 \cdot 4H_2O$ (3 mg, 0.01 mmol), H_2pip (2.2 mg, 0.01 mmol), and 1,2-di(pyridin-4-yl)ethane (bpe) (1.8 mg, 0.01 mmol) were taken in a 8 mL scintillation vial. Three milliliters of dimethylformamide (DMF) was then added. The mixture was stirred for 10 min to give a clear solution.

Subsequently, the reaction vial was capped and placed in a programmable oven and heated at $90^\circ C$ for 2 days and cooled to room temperature at a rate of $0.15^\circ C/min$. Colorless crystals (2.5 mg, 61%) of the product were collected by filtration and washed with DMF (3×5 mL). IR spectra (ν/cm^{-1}) 3401, 2937, 2865, 1600, 1548, 1436, 1300, 1246, 1218, 1021, 974, 862, 787, 737, 681, 617, 525. Elemental analysis of activated sample: Anal. Calcd for $C_{23}H_{18}O_5N_2Cd$; [$Cd(pip)(bpe)$] C, 53.66; H, 3.52; N, 5.44. Found: C, 53.75; H, 3.34; N, 5.62.

Synthesis of Metal Nanoparticles@MOFs. Activated MOFs were used for the preparation of MOF supported MNPs. A wet chemical method was employed to generate MNPs. In the case of MOF-3, the MNP loading amount was gradually increased starting from 5 wt % until it got saturated. For others MOFs, a constant amount of metal ion precursor in methanol was used, and the amount of Pd adsorbed into those was estimated from ICP-MS. The maximum loading amount was reproduced for bulk scale preparation.

5 wt % Pd@MOF-3. To 5 mg of the activated MOF-3 in 4 mL of methanol, 0.42 mg (2.4×10^{-3} mmol) of $PdCl_2$ in 1 mL of methanol was added slowly. The mixture was kept stirring at room temperature for 30 min to adsorb Pd^{2+} ions into the MOF. During this time, the dark orange color of the supernatant (due to $PdCl_2$) turned colorless, and the MOF turned to brown from colorless. Subsequently, 0.45 mg (1.2×10^{-2} mmol, 5 equiv with respect to $PdCl_2$) of $NaBH_4$ was added with constant stirring for another 1 h. During this period, the mixture turned black indicating the formation of Pd NPs. Finally, the mixture was filtered and washed several times with fresh methanol. The solid material was then dried under vacuum.

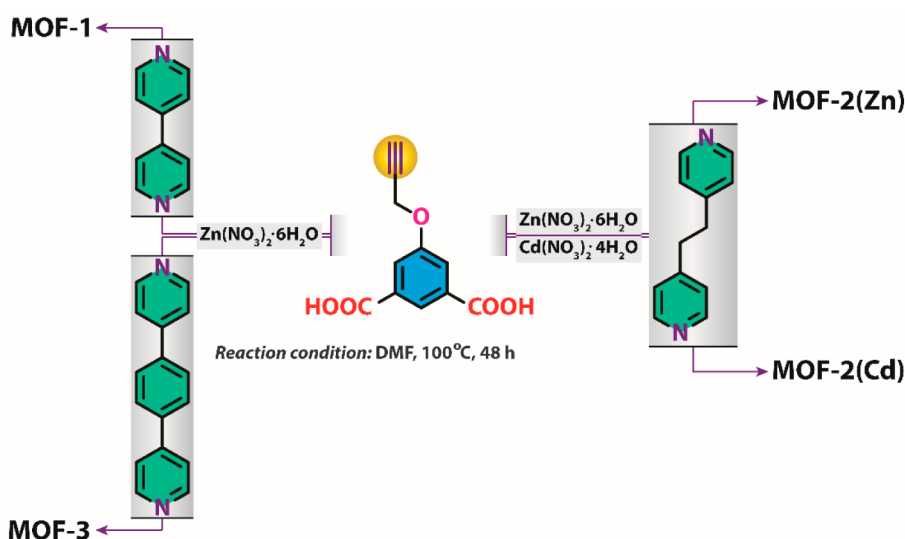
Thirty wt % Pd@MOF-3. This was also prepared in a similar method as described above using 2.5 mg (1.4×10^{-2} mmol) of $PdCl_2$ added in 5 mg of MOF in methanol. Subsequently, 2.7 mg (7.05×10^{-2} mmol, 5 equiv with respect to $PdCl_2$) of $NaBH_4$ was added for the reduction of Pd^{2+} ions.

Control Experiments. 5 wt % Pd@MOF-A. To 5 mg of activated MOF-A [$Zn(bip)(dpb)$] (where bip corresponds to 5-(benzyloxy)-isophthalate) in 4 mL of methanol, 0.42 mg (2.4×10^{-3} mmol) of $PdCl_2$ in 1 mL of methanol was added slowly. The mixture was kept stirring at room temperature for 30 min. Subsequently, 0.45 mg (1.2×10^{-2} mmol, 5 equiv with respect to $PdCl_2$) of $NaBH_4$ was added with constant stirring for another 1 h. During this period, the mixture turned dark gray due to the formation of Pd nanoparticles. Finally, the mixture was filtered and washed several times with fresh methanol. The solid material was then dried under vacuum.

General Procedure for the Heck-Coupling Reactions of Aryl Iodides. To a two-necked 50 mL round-bottomed flask, an aryl iodide (2 mmol), an alkene (4 mmol, 2 eqv.), tetrabutylammonium acetate (TBAA, 0.4 mmol, 0.2 eqv.), triethylamine (6 mmol, 3 eqv.), and Pd@MOF-3 (10 mg, 1.25 mol % Pd) were added. The reaction vessel was degassed three times and subsequently filled with nitrogen gas. To this, anhydrous 1-butanol (10 mL) was added through a syringe. Then, the resulting suspension was stirred under nitrogen atmosphere at $80^\circ C$ for 24 h. After cooling to room temperature, the catalyst was separated by filtration, and then, the solvent was evaporated under reduced pressure. The residue obtained was purified by column chromatography over silica gel eluting with hexane/ethyl acetate to afford the corresponding products.

General Procedure for the Heck-Coupling Reaction of Aryl Bromides. The corresponding aryl bromide (2 mmol), alkene (4 mmol, 2 eqv.), tetrabutylammonium acetate (TBAA, 0.4 mmol, 0.2 eqv.), sodium acetate (6 mmol, 3 eqv.), and Pd@MOF-3 (10 mg, 1.25

Scheme 2. Schematic Representation of the Preparation of Different Porous MOFs Depending on the Pillar Height of the Bipyridyl Ligands



mol % Pd) were taken in a 50 mL two-necked round-bottomed flask. Then, the reaction flask was degassed three times and subsequently filled with nitrogen gas. To this, anhydrous dimethylformamide (DMF, 10 mL) was added through a syringe. The resulting suspension was stirred under nitrogen atmosphere at 120 °C for 24 h. After cooling to room temperature, the catalyst was separated by filtration, and then, the solvent was evaporated under reduced pressure. The residue obtained was purified by column chromatography over silica gel eluting with hexane/EtOAc to afford the corresponding products.

General Procedure for the Alkene Hydrogenation Reaction. To a hydrogenation flask, an alkene (2 mmol) was dispersed in anhydrous ethanol (15 mL). To this, 5 mg of Pd@MOF-3 (0.6 mol %) was added. Subsequently, the mixture was sonicated for a few minutes to ensure that the catalyst homogeneously dispersed into ethanol. Finally, the reaction mixture was fixed in a hydrogenation apparatus with constant shaking at 4 bar pressure and 60 °C temperature. Initially, pressure, temperature, and catalyst amount were optimized to obtain the maximum hydrogenation product using styrene as a substrate. The reaction time was also optimized for styrene with above-mentioned pressure and temperature for 5 h. The same reaction conditions were followed for all other starting materials. After the specified time, the catalyst was separated by filtration, and then, ethanol was removed under reduced pressure. The conversion/purity of the crude products was estimated/judged by NMR spectroscopy. Hydrogenation using other Pd@MOFs was carried out in a similar way.

Reusability of the Catalyst. Iodobenzene (10 mmol), methyl acrylate (15 mmol, 1.5 eqv.), tetrabutylammonium acetate (TBAA, 2 mmol, 0.2 eqv.), triethylamine (15 mmol, 1.5 eqv.), and Pd@MOFs (50 mg) were taken in a 50 mL reaction vessel. The reaction mixture was degassed several times and finally filled with nitrogen gas. To this, anhydrous 1-butanol (30 mL) was added through a syringe. The resulting mixture was stirred under nitrogen at 80 °C for 24 h. After cooling down to room temperature, the catalyst was filtered, washed several times with ethyl acetate, and then dried under vacuum. The recovered catalyst was used again another three times for the same reaction using the same procedure. Similarly, for hydrogenation the recovered catalysts were used for five different cycles, and in every case, the conversion was estimated from NMR spectroscopy. The stability of the recovered catalysts after reactions was judged by TEM and PXRD analysis.

RESULTS AND DISCUSSION

Synthesis. In general, a well-defined functionalized pore or channel of MOFs offers potential application for sensing and separation.¹⁵ In this context, the 5-(prop-2-yn-1-yloxy)-

isophthalate (*pip*) ligand has been used for the preparation of four MOFs along with different dinitrogen linkers *bpy*, *bpe*, and *dpb*. The *pip* ligand has two distinct functionalities: isophthalate (*iph*) and a functionalized ethynyl moiety. The *iph* unit was used for the generation of co-ordination polymer backbone with metal ion connectors; however, the ethynyl functionality was introduced with the intention to stabilize noble metal ions inside the pore through the π -donor and π -acceptor interaction. Dinitrogen linkers of different heights were used as an interlinking unit to gradually enhance the porosity in the three-dimensional (3D) networks. Also, they will certainly provide variable pore size in the MOFs, which may give an opportunity to study pore size dependent size distributions of metal nanoparticles as well as NP loading amount. Thus, solvothermal reactions of *pip* along with bipyridyl ligands, such as *bpy*, *bpe*, and *dpb*, in dimethylformamide (DMF) with $\text{Zn}(\text{NO}_3)_2 \cdot 6\text{H}_2\text{O}$ at 100 °C for 48 h resulted in MOF-1, MOF-2(Zn), and MOF-3, respectively. The reaction of *pip* and *bpe* with $\text{Cd}(\text{NO}_3)_2 \cdot 4\text{H}_2\text{O}$ under similar reaction conditions yielded MOF-2(Cd). All of the MOFs were isolated in highly crystalline form with excellent yields (Scheme 2). MOF-2(Zn) and MOF-2(Cd) are isostructural, and also, our preliminary experiments suggest that their behavior does not vary considerably for stabilization of Pd NPs. Therefore, in the present study, MOF-1, MOF-2(Cd), and MOF-3 have been highlighted for Pd NPs loading and their catalytic applications.

Single Crystal X-ray Structures. The single-crystal X-ray diffraction analyses revealed that MOF-1, MOF-2(Zn), and MOF-2(Cd) were crystallized in a monoclinic crystal system with $P2_1/c$ (MOF-1) and $C2/c$ (MOF-2) space groups (Figure 1). All of the MOFs form three-dimensional (3D) networks with channel-like pores. Though as synthesized MOF-3 was obtained as a highly crystalline material, several attempts remained unsuccessful to obtain better single crystal data. Fortunately, the PXRD pattern indicated that the as-synthesized MOF-3 has structural arrangement similar to that of MOF-1 and MOF-2 (Figure 2a).

The crystal structures of MOF-2(Zn) and MOF-2(Cd) revealed that they are isostructural to each other and possess similar porosity. It was also observed that in every MOF the void channels are occupied by guest solvent molecules such as

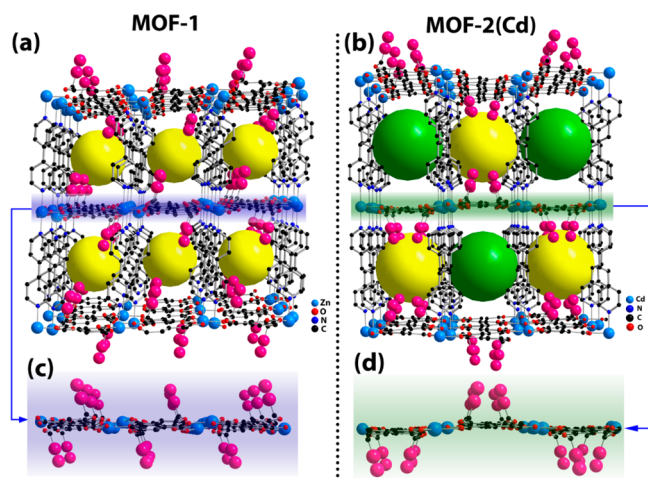


Figure 1. (a and b) Crystal structures of MOF-1 and MOF-2(Cd); the extended three-dimensional network of the MOFs showing channel like pores. For MOF-1, each pore is decorated by functionalized ethynyl moieties highlighted by yellow balls. In MOF-2(Cd), the ethynyl moieties are located in alternative pores shown as yellow and green balls. (c and d) Highlighted two-dimensional layered network involving *iph* units of *pip* and Zn^{2+} or Cd^{2+} ions. The ethynyl moieties are highlighted in pink.

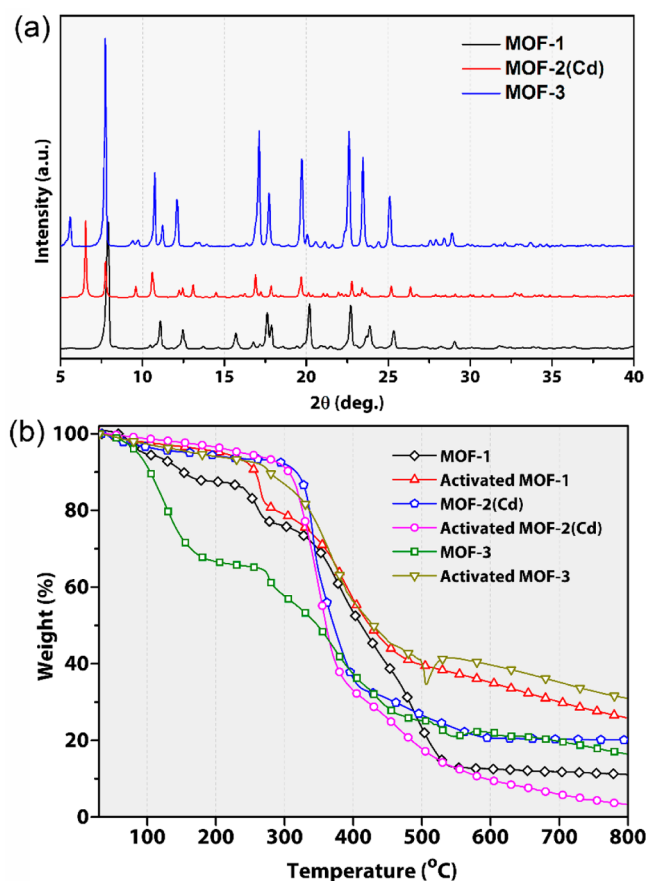


Figure 2. (a) PXRD patterns of as-synthesized MOFs-1-3. (b) TGA plots of MOFs 1–3 along with their activated forms.

DMF and H_2O . In all of the frameworks, as expected the *iph* moieties of the ligands formed a two-dimensional layered network connecting distorted octahedral Zn^{2+} or Cd^{2+} ions. The equatorial sites of each Zn^{2+} or Cd^{2+} ion are coordinated

by four O atoms of three different *iph* units. In every case, the ethynyl moieties resided above and below the 2D layered networks (Figure 1c and d). These 2D layers are interconnected to each other by either *bpy* (MOF-1) (Figure 1) or *bpe* (MOF-2) or *dpb* (MOF-3) linkers via coordination at the axial positions of the Zn^{2+} or Cd^{2+} ions to render 3D MOFs with huge porous channels. The representative crystal structures of MOF-1 and MOF-2(Cd) are given in Figure 1. Interestingly, as anticipated the ethynyl moieties are pointed toward the interior of the MOFs pores (Figure 1a or b). It was observed that in MOF-1 the ethynyl moieties are present in every channel; however, in MOF-2 those are located in alternate channels.

Powder X-ray Diffraction (PXRD) and Thermogravimetric Analysis (TGA). Powder X-ray diffraction (PXRD) and thermogravimetric analysis (TGA) were carried out to understand the phase purity and thermal stability of the MOFs. A comparison of the simulated PXRD patterns of MOF-1, MOF-2, and MOF-3 with the as-synthesized material indicated that all of the MOFs were prepared in single phase in highly pure form (Supporting Information). Moreover, a comparison of the PXRD patterns of as-synthesized MOF-3 with that of MOF-A indicated that MOF-3 also adopts molecular structure similar to it (Supporting Information). Although MOF-1, MOF-2, and MOF-3 have similar structures, considerable shifts in the PXRD patterns were mainly due to the increase of unit cell dimension from MOF-1 to MOF-2 to MOF-3 depending upon pillars. The PXRD patterns of the activated (desolvated) samples indicated that the MOFs' networks are extremely stable even after the removal of the solvent molecules from the pores.

Thermogravimetric analysis (TGA) revealed an almost constant weight loss for all of the MOFs up to 200 °C, which was attributed to the removal of guest water and DMF (Figure 2b). All of the MOFs have significant thermal stability up to ~250 °C. The stability of the activated samples had been demonstrated by TGA, which displayed their thermal stabilities similar to that of as-synthesized samples. Since one of the requirements of heterogeneous catalysis is their high thermal stability, these could be useful several times. Thus, the high thermal stability of the current MOFs meets the demands of potential application in heterogeneous catalysis.

Loading of Pd Nanoparticles. Here, we have adopted a solvent infiltration method to load MNPs into MOFs in stepwise manner starting from corresponding metal ion precursors. The NP preparation involves two distinct steps. First, adsorption of metal ions into MOFs interior second, reduction of metal ions by $NaBH_4$ to their respective NPs (Scheme 1). The MOFs were initially activated to remove all of the solvent molecules from the pores. The supported Pd NPs were synthesized from the $PdCl_2$ precursor in methanol by wet chemical reduction using $NaBH_4$. To establish the two-step mechanism of the Pd NPs formation, the reactions were carried out stepwise. Initially, the metal ion precursor in methanol was added to the activated MOF-3 crystals. Interestingly, the bright orange color of the $PdCl_2$ solution disappeared gradually during 2 h of time, and simultaneously, the colorless MOF-3 turned brown indicating the adsorption of Pd^{2+} ions into the MOF (Figure 3). The adsorption process was significantly facilitated by stabilization of Pd^{2+} ions inside the MOF's pores through the Pd-ethynyl interaction. To get a clear idea about this adsorption process, SEM energy dispersive X-ray (EDX) mapping was carried out using Pd^{2+} adsorbed MOF-3. Figure

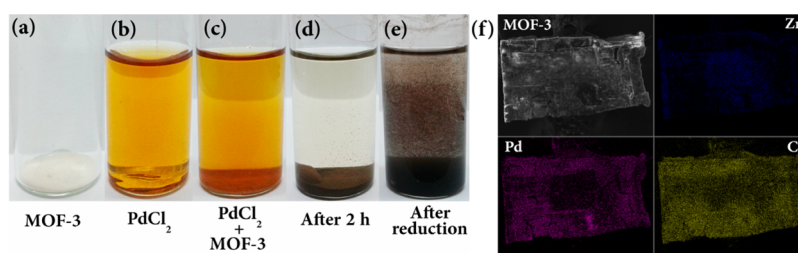


Figure 3. Synthesis of Pd NPs in two sequential steps. (a) MOF-3, (b) PdCl₂ solution in methanol, (c) MOF-3 and PdCl₂ mixed together, and (d) visual color change after 2 h. The supernatant becomes colorless from orange, and MOF-3 crystals turned brown. (e) Reduction of Pd²⁺ ions to Pd NPs by NaBH₄. (f) SEM-EDX mapping of PdCl₂ adsorbed MOF-3.

3f indicates that the Pd²⁺ ions are adsorbed homogeneously throughout the entire MOF-3. Subsequent reduction of Pd²⁺ ions by NaBH₄ yielded Pd NPs. It is worth mentioning here that unlike H₂AuCl₄ adsorption reported earlier by us,¹⁴ the same concentration of PdCl₂ adsorbed at a much slower rate compared to that of the H₂AuCl₄ solution. Also, the adsorption reached a steady-state value at a much lower concentration of Pd²⁺ compared to that of Au³⁺ ions which is mainly due to the fact that Au³⁺ ions have stronger electronic interaction with ethynyl compared to that of the Pd²⁺ ion.^{13a} This fact was reflected in the lower loading amount of Pd into MOF-3 compared to that of Au. In this case, it was possible to load only ~27 wt % Pd NPs without any agglomeration in contrast to 50 wt % Au NPs using the same MOF.

To determine the maximum loading capability of the MOFs without altering the monodispersity and particle size of the NPs, the MNP loading was increased gradually starting from 5 wt % using MOF-3 until the particles start to agglomerate. In this process, up to ~27 wt % Pd (inductively coupled plasma mass spectroscopy (ICP-MS) loading was achieved (the exact loading is 26.9 ± 1.2 wt %). In a similar procedure, about ~10 and 12.5 wt % of Pd NPs (ICP-MS experiment indicated the exact amounts were 9.8 ± 1.1 wt % and 12.5 ± 1.6 wt %, respectively) loaded into MOF-1 and MOF-2(Cd), respectively.

The TEM characterization of the Pd@MOF-3 is depicted in Figure 4. It is evident from the TEM bright field (TEM-BF) image that Pd NPs are homogeneously dispersed in MOFs with a mean particle diameter of 2.8 ± 0.3 nm as estimated from particle size distribution. Considering the pore diameter of the MOF-3, it can be concluded that the bigger particles with a diameter more than 2.77 nm are presumably located in a distorted MOF-3 surface or at the outer surface of the MOF crystals but stabilized by the surface ethynyl groups. Similar observations are also reported in the preparation of MNPs in zeolitic materials or in other reported MOFs.¹⁶ We found it extremely difficult to carry out HRTEM measurements on the small sized (<3 nm) particles due to sample charging under the electron beam. Thus, comparatively larger particles were selected for the HRTEM image. The presence of Pd NPs in MOF-3 was thus confirmed by the HRTEM image (Figure 4d) as the lattice spacing $d = 2.24 \text{ \AA}$ of (111) plane of *fcc* Pd is consistent with the reported value of Pd(0) NPs. Also in the STEM dark field image, the brighter spots are attributed to the Pd NPs, which are homogeneously dispersed into the MOF matrix. Similarly, Pd@MOF-1 and Pd@MOF-2(Cd) were also characterized by the TEM techniques which are compiled in the Supporting Information. Importantly, as observed in the Pd@MOF-3, the particles are also homogeneously distributed

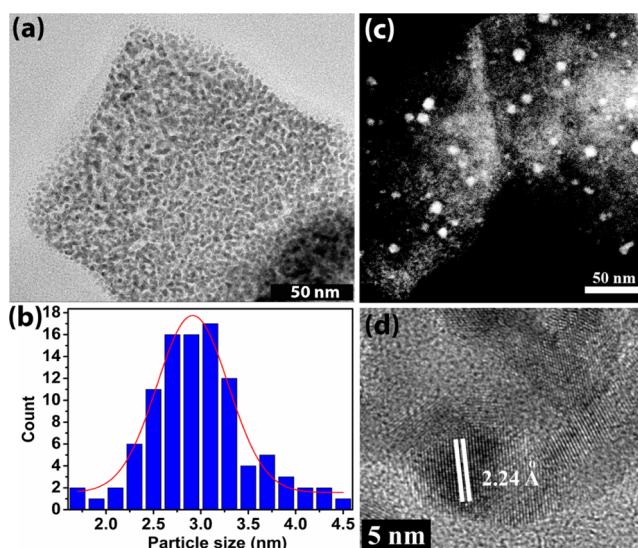


Figure 4. Twenty-seven wt % Pd loading in MOF-3. (a) Bright-field TEM image showing that the Pd NPs are homogeneously loaded in MOF-3. (b) Corresponding Pd NPs size distribution histogram. (c) STEM-HAADF image of the Pd@MOF-3. (d) HRTEM image.

into MOF-1 and MOF-2(Cd) with mean particle diameters 1.5 ± 0.2 nm and 2.1 ± 0.3 nm, respectively.

PXRD has been an excellent tool to confirm the NPs formation and stability of MOFs after NP loading. In this case, representative PXRD patterns of PdCl₂@MOF-1 and Pd@MOF-1 are given in Figure 5 compared with that of activated MOF-1. The crystallinity of MOF-1 remained intact even after the loading of PdCl₂ and its reduction to Pd NPs, although

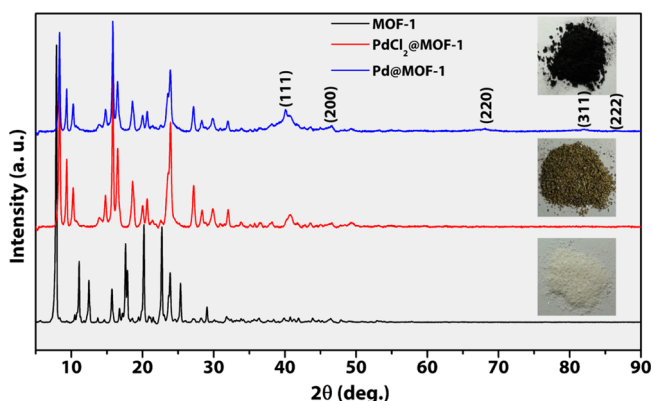


Figure 5. Comparison of PXRD patterns of MOF-1, PdCl₂@MOF-1, and Pd@MOF-1 along with their visual color change after each step.

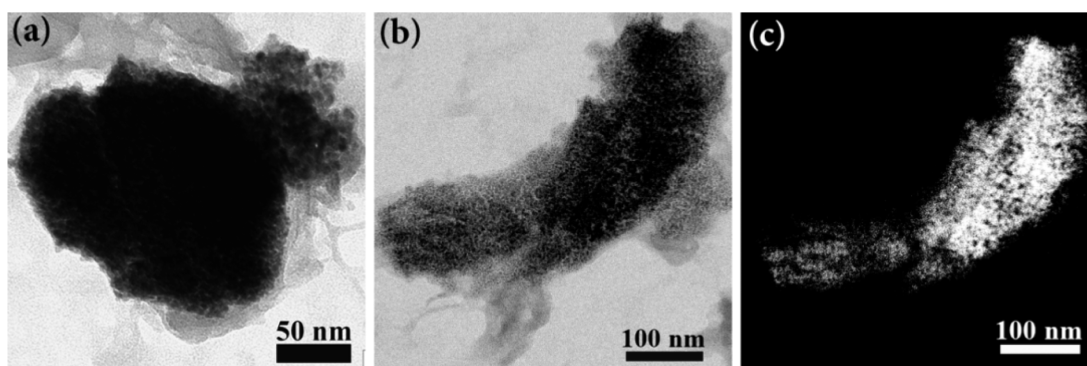


Figure 6. Five wt % Pd loading in MOF-A. (a) Bright-field TEM image showing the polydispersity of Pd NPs and their location mostly at the surface of the MOF-A. (b) STEM bright field and (c) STEM-HAADF images of the Pd@MOF-A.

there was a shift of the peaks after the adsorption of PdCl₂. Along with their PXRD patterns, the visual color change of the MOF-1 crystals after each step was also provided in Figure 5. The colorless MOF-1 changes to golden yellow after the adsorption of PdCl₂, while retention of crystallinity was clearly evident. Finally, the color changes to black after reduction indicating the formation of Pd NPs. The sharp diffraction peaks at low angle regions are due to MOF-1 itself, while the high angle broad peaks are due to Pd NPs. Particularly, peaks at 39.8, 46.3, 67.6, 81.2, and 85° in the PXRD pattern are characteristics of (111), (200), (220), (311), and (222) planes, respectively, corresponding to *fcc* Pd NPs. The formation of Pd⁰ NPs was also confirmed by XPS analysis. The peaks at 340.7 and 335.3 eV are due to the binding energy corresponds to 3d_{3/2} and 3d_{5/2} levels, respectively, which indicates the formation of Pd⁰ NPs (Supporting Information).

Control Experiment. To establish whether the ethynyl moieties have any direct influence or the framework itself is responsible to stabilize Pd NPs, a structurally similar MOF (MOF-A) containing a functionalized phenyl moiety instead of the ethynyl group has been used to stabilize the same metal NPs.¹⁷ Interestingly, in the controlled experiments, loading of only 5 wt % Pd into MOF-A in a similar process indicated that MOF-A cannot stabilize either metal ions or the metal NPs. In Figure 6, the TEM images of Pd@MOF-A show that the Pd NPs are mostly agglomerated and located on the surface of MOF-A crystals. The STEM images also showed the agglomerated nature of Pd NPs and their location on the surface of MOF-A. However, loading of NPs did not cause any decomposition of the MOF-A, which was established by the PXRD analysis. Thus, the above results indicate that the ethynyl functionality had a substantial role in the stabilization of Pd NPs.

Pillar Height Dependent Particle Size. Recently, enormous attention has been paid to the synthesis of MOF supported metal NPs. However, the systematic studies on the role of MOF pore size on metal NPs are extremely rare. More importantly, size dependent catalytic activities of the metal NPs were also not explored well. The present MOFs offer an ample opportunity to study this fact. Porosity as well as solvent accessible volume of the MOFs was increased from MOF-1 to MOF-3 as observed from the single crystal X-ray structure depending upon the interlinking dinitrogen pillar.

Also, the NP size distribution as obtained from TEM experiments is in accordance with the porosity of the MOFs. The mean particle diameters are 1.5, 2.1, and 2.8 nm, respectively, when they are loaded into MOF-1, MOF-2(Cd),

and MOF-3 (Table 1). However, the mean particle size observed in the former two MOFs are not in similar to their

Table 1. Pd Loading Amount and Their Corresponding Sizes When Those Are Loaded into Different MOFs

Pd@MOFs	loading amount	size of the Pd NPs
Pd@MOF-1	9.7 ± 1.1 wt %	1.5 ± 0.2 nm
Pd@MOF-2(Cd)	12.5 ± 1.6 wt %	2.1 ± 0.3 nm
Pd@MOF-3	26.9 ± 1.2 wt %	2.8 ± 0.3 nm

pore diameter, which is smaller than the particle size. The particles smaller than pore diameters are expected to be mainly located inside the pore, and the bigger particles are most probably stabilized on the surface by ethynyl groups.

However, in the case of MOF-3, because of larger pillar height and comparatively higher surface area, it was expected that the particles are located mainly inside the pore. Therefore, nitrogen gas adsorption was performed for MOF-3 and Pd@MOF-3 at 77 K to find out their exact surface area and pore diameter. The surface area reduced significantly from 54.8 m²/g to 21.7 m²/g upon loading of Pd NPs into MOF-3 (Supporting Information). Probably, the pores of the MOF-3 are blocked by Pd NPs which causes significant reduction of the surface area. Although the mean particle diameter of the Pd NPs (2.8 nm) at MOF-3 is bigger than the pore dimension of MOF-3, it is expected that smaller particles are mainly located inside the pores and that the bigger particles are mainly outside the pore. MOF-1 and MOF-2 do not show any nitrogen adsorption behavior, which indicates that these two MOFs have less porosity compared to that of MOF-3.

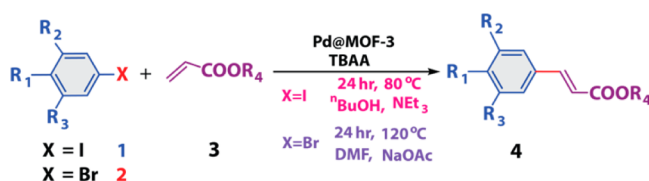
The effect of pore size and surface area of the MOFs are also reflected on the Pd loading amount. Initially, 30 wt % Pd was attempted to load into MOF-1, MOF-2(Cd), and MOF-3 via the two-step mechanism as mentioned earlier. The amount of Pd NPs loaded into the MOFs (calculated amount from ICP-MS) are ~10 wt %, ~12.5 wt %, and ~27 wt %, respectively, which is in accordance with the surface area of the respective MOFs. The more porous MOFs (MOF-3) can stabilize larger amounts of NPs without agglomeration compared to the less porous MOFs. Therefore, the current studies reveal that the NP sizes and loading amounts are highly dependent on the porosity of the MOFs. Table 1 summarizes Pd NP loading amounts and sizes on different MOFs.

Heck-Coupling Reactions. Recently, Pd-catalyzed C–C coupling reactions such as Suzuki–Miyaura, Ullmann, Heck, and Sonogashira reactions have evolved as the most important

and useful reactions for traditional organic synthesis.¹⁸ Particularly, Heck-coupling reactions were widely carried out using homogeneous Pd-catalysts, but their potential applications in the chemical industry are still limited due to difficulties related to their efficient recovery from the reaction mixtures. However, heterogeneous Pd-catalysts could be a promising solution to this problem. In this current study, we anticipated that the high loading and small size of the Pd NPs into MOFs could be ideal for catalysts for the Heck-coupling reactions. Therefore, several Heck-coupling reactions were performed in the presence of Pd@MOFs involving aryl iodides or bromides and alkenes.

Initially, all of the reactions were performed using representative 1.25 mol % of the Pd@MOF-3 catalyst. Several electron-donating or electron-withdrawing aryl iodides and bromides afforded cross-coupling products with excellent yields. Cross-coupling products involving acryl esters and styrene are separately listed in Tables 2 and 3, respectively.

Table 2. Catalytic Heterogeneous Heck-Coupling Reactions with Aryl Halides and Acrylic Esters Using Pd@MOF-3

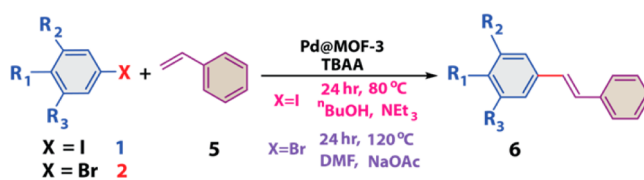


entry no.	1 or 2 (R ₁ , R ₂ , R ₃)	3 (R ₄)	4	yield [%]
1	1 (H, H, H)	3 (Me)	4a	99
2	1 (H, H, H)	3 (Et)	4b	99
3	1 (H, H, H)	3 (^t Bu)	4c	99
4	2 (H, H, H)	3 (Me)	4d	95
5	1 (Me, H, H)	3 (Me)	4e	98
6	2 (Me, H, H)	3 (Me)	4f	94
7	1 (H, Me, Me)	3 (Me)	4g	98
8	1 (H, Me, Me)	3 (Et)	4h	98
9	1 (H, Me, Me)	3 (^t Bu)	4i	97
10	2 (H, Me, Me)	3 (Me)	4j	93
11	1 (OMe, H, H)	3 (Me)	4k	95
12	2 (OMe, H, H)	3 (Me)	4l	92
13	1 (H, CO ₂ Me, CO ₂ Me)	3 (Me)	4m	87
14	1 (H, Me, CO ₂ Me)	3 (Me)	4n	91

Interestingly, two different reaction conditions were employed for aryl iodides and bromides depending on their reactivity. Although the less reactive aryl bromide generally required somewhat drastic conditions, its conversion remained excellent (90–99%) under the present reaction conditions using the Pd@MOF-3 catalyst. The yields of the reactions were estimated from the NMR spectra. It is noted that the reaction rate is highly dependent on the catalyst amount (mol % of Pd); however, in the presence of a small catalyst amount the reactions proceeded smoothly but needed longer time for full conversion.

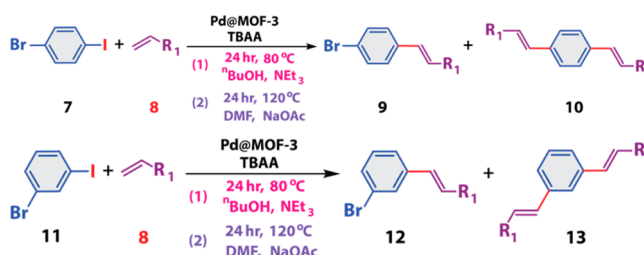
Selectivity between Iodide and Bromide. The different reactivities of aryl iodides and bromides gave an opportunity to convert selectively the former in the presence of the latter. To establish this fact, two reactants containing both iodide and bromide were chosen (Table 4). When the reactions were carried out at 80 °C in *n*-butanol for 24 h, only iodides underwent the cross-coupling reaction. However, when similar reactions were performed at 120 °C in DMF for 24 h, both

Table 3. Catalytic Heterogeneous Heck-Coupling Reactions with Aryl Halides and Styrene Using Pd@MOF-3



entry no.	1 or 2 (R ₁ , R ₂ , R ₃)	5	6	yield [%]
1	1 (H, H, H)	5	6a	98
2	2 (H, H, H)	5	6b	94
3	1 (Me, H, H)	5	6c	97
4	2 (Me, H, H)	5	6d	95
5	1 (H, Me, Me)	5	6e	98
6	2 (H, Me, Me)	5	6f	94
7	1 (OMe, H, H)	5	6g	92
8	2 (OMe, H, H)	5	6h	88
9	1 (H, CO ₂ Me, CO ₂ Me)	5	6i	82
10	1 (H, Me, CO ₂ Me)	5	6j	87

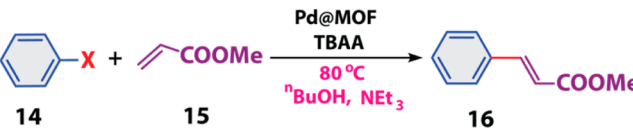
Table 4. Selective Catalytic Heterogeneous Heck-Coupling Reactions Using Pd@MOF-3 for Reactants Containing Both Iodo- and Bromo-Groups



entry no.	condition	Ar-X	8 (R ₁) (4 eqv.)	9 (yield)	10 (yield)
1	(1)	7	8 (CO ₂ Me)	9a (95%)	10a (2%)
2	(2)	7	8 (CO ₂ Me)	9a (0%)	10a (96%)
3	(1)	7	8 (Ph)	9b (93%)	10b (3%)
4	(2)	7	8 (Ph)	9b (0%)	10b (87%)
entry no.	condition	Ar-X	8 (R ₁) (4 eqv.)	12 (yield)	13 (yield)
1	(1)	11	8 (CO ₂ Me)	12a (92%)	13a (3%)
2	(2)	11	8 (CO ₂ Me)	12a (0%)	13a (94%)
3	(1)	11	8 (Ph)	12b (88%)	13b (4%)
4	(2)	11	8 (Ph)	12b (0%)	13b (85%)

iodides as well as bromides gave coupling products. Thus, these catalysts provide an opportunity to tune the product selectivity by tuning a simple reaction parameter, which is essential for selective organic transformation.

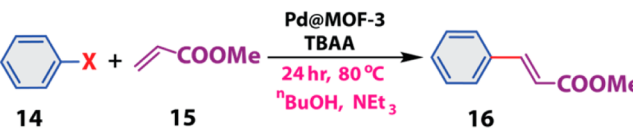
Effect of the Size of the Nanoparticles. To understand the role of NP size on the catalytic activity, a representative Heck-coupling reaction was carried out using iodobenzene and methyl acrylate in the presence of Pd NPs at different MOFs (Table 5) with fixed catalyst amount (in terms of mol %). Size of the Pd NPs was highly dependent on the porosity of the MOFs. In the present case, the Pd NP size increased from 1.5 to 2.8 nm in MOF-1 to MOF-3, respectively, depending on the porosity of the MOFs. It is expected that size of the NPs should have a role in the conversion rate of the catalytic reaction if the reactions are monitored with time. In this particular case, even though the final yields of the reactions were similar after a longer time period (24 h), a higher reaction rate was noted during the initial period (6 h) in the case of smaller sized

Table 5. Catalytic Reactions Using Pd NPs @ Various MOFs Having Different Particle Sizes


entry no.	Pd@MOF	size of the NPs	Ar-X	time [%]	
				6 h (yield)	24 h (yield)
1	Pd@MOF-1	1.5 nm	Ph-I	16 (74%)	16 (99%)
2	Pd@MOF-2(Cd)	2.1 nm	Ph-I	16 (72%)	16 (99%)
3	Pd@MOF-3	2.8 nm	Ph-I	16 (62%)	16 (99%)

particles as catalysts. This could be rationalized by the fact that smaller particles possess a higher fraction of surface atoms (and thus the catalytically active site) compared to that of their larger counterpart.

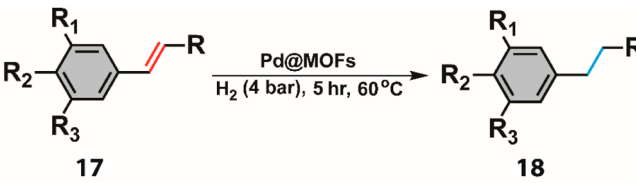
Reusability of the Catalyst. The recyclability of the Pd@MOF-3 catalyst was examined by carrying out a similar reaction using iodobenzene and methyl acrylate (Table 6). The results

Table 6. Recyclability Test of the Pd@MOF-3 Catalyst in the Heck-Coupling Reaction Involving Iodobenzene and Methylacrylate


cycles	Ar-X	15	(16) yield [%]
1	Ph-I	15	99
2	Ph-I	15	98
3	Ph-I	15	96
4	Ph-I	15	90

demonstrated that the catalyst can be recycled at least four times without significant loss of catalytic activity. The stability of the catalyst was further confirmed by the TEM imaging and PXRD of the recovered catalyst (Supporting Information). The TEM images of the recycled material showed that NPs are still highly dispersed into MOFs. The PXRD pattern of the corresponding recovered catalyst also indicated that the crystallinity and stability of the MOF-3 was maintained after four different cycles, though the peak intensity gradually decreased. That might be due to the degradation of structural regularity caused by repetitive exposure of the Pd@MOF-3 catalyst to the basic conditions. A Pd leaching test was carried out to get an idea as to whether Pd was coming out of the MOFs during reactions. In the absence of reactants, a mixture of Pd@MOF-3 and triethylamine or sodium acetate was heated with stirring at 80 °C in *n*-butanol for 24 h. The filtrate of the hot reaction mixture was used for the catalytic reaction of iodobenzene and methyl acrylate. There was no conversion of the reaction which indirectly confirmed that Pd did not leach out into the filtrate. This study also indicated the strong interaction between Pd and MOFs (predominantly the Pd-ethynyl interaction), and it is even quite stable under reaction conditions.

Pd@MOF Catalyzed Hydrogenation. Stabilized Pd NPs have been used for heterogeneous catalytic hydrogenation of unsaturated organic molecules in the recent past.¹⁹ However, the activity and efficiency of these materials are highly dependent on their size, loading amount on the substrate, and the nature of the stabilizer. Ideally, the high loading amount of Pd NPs into MOFs increases the high adsorption of hydrogen gas, which can facilitate the facile hydrogenation of alkenes. Initially, the reaction was performed under mild conditions, that is, at room temperature in chloroform using Pd@MOF-3. Because of the low conversion rate, finally the reaction was optimized, and all the other reactions were carried out at 60 °C and 4 atm pressure in ethanol for 5 h (Table 7).

Table 7. Catalytic Hydrogenation of Alkenes Using the Pd@MOF-3 Catalyst under Hydrogen Gas


entry no.	17 (R)	17 (R ₁ , R ₂ , R ₃)	18	yield [%]
1	17 (H)	17 (H, H, H)	18a	99
2	17 (H)	17 (H, Me, H)	18b	99
3	17 (H)	17 (H, Cl, H)	18c	99
4	17 (Ph)	17 (H, H, H)	18d	95
5	17 (Ph)	17 (H, Me, H)	18e	98
6	17 (Ph)	17 (Me, H, Me)	18f	94
7	17 (Ph)	17 (H, Br, H)	18g	98
8	17 (Ph)	17 (Br, H, H)	18h	98
9	17 (COOMe)	17 (H, H, H)	18i	97
10	17 (COOMe)	17 (Me, H, Me)	18j	93
11	17 (COOMe)	17 (H, Br, H)	18k	95
12	17 (COOMe)	17 (Br, H, H)	18l	92
13	17 (COOMe)	17 (CO ₂ Me, H, CO ₂ Me)	18m	87

Under this particular reaction condition, the conversion was excellent, and more than 90% yield was achieved. Irrespective of reaction conditions, in polar protic solvent such as ethanol the reactions were completed faster. The rate of the representative catalytic hydrogenation of styrene remained the same irrespective of Pd NPs sizes when they were loaded into three different porous MOFs described here. This is most probably due to close particle size distribution which did not affect the reaction rate much.

Reusability of the Pd@MOFs Catalyst after Hydrogenation. Reusability of the Pd@MOF-3 catalyst was tested for the hydrogenation of styrene several times using the recovered catalyst under similar reaction conditions as mentioned earlier (Table 8). The results demonstrated that

Table 8. Recyclability Test for the Hydrogenation of Styrene in Ethanol Using Pd@MOF-3

cycles	pressure (atm), temperature (°C)	time (h)	conversion (%)
1	4, 60	6	99
2	4, 60	6	97
3	4, 60	6	94
4	4, 60	6	93
5	4, 60	6	87

Pd@MOF-3 can be used for at least five different cycles without much loss of catalytic activity. The TEM images of the recovered catalyst indicate that the Pd NPs are homogeneously dispersed even after the catalytic reactions. Also, a sharp PXRD pattern of the recycled catalyst suggested that MOF-3 remained intact under the reaction conditions (Supporting Information). The Pd leaching test was also performed to understand whether Pd NPs were coming out of the MOFs during hydrogenation reactions. Typically, after hydrogenation the whole reaction mixture was filtered, and ICP-MS analysis was carried out to find the Pd in the filtrate with respect to the standard solutions. Note that no significant signal was observed corresponding to Pd. Therefore, Pd was not leaching out of the MOF-3, and it also established that Pd NPs have a strong interaction with MOFs.

High Temperature Stability of the Pd@MOFs Catalyst. Recently, considerable efforts have been devoted toward the high temperature stability of the catalyst such that those can be used for organic transformations at elevated temperature.²⁰ Generally, organic capping-agent stabilized NPs are often limited for high temperature catalytic reactions due to NPs agglomeration. However, owing to the inherent high thermal stability of the MOFs, NPs stabilized by those are expected to have higher thermal stability and therefore can be useful at elevated temperature. The thermal stability of representative Pd@MOF-3 was checked by a thermal annealing process at 150 °C followed by TEM analysis. In the typical annealing process, a sealed sample of Pd@MOF-3 in a glass tube was heated under vacuum in a programmable oven for 3 h at 150 °C. After cooling down to room temperature, the sample was prepared for TEM analysis. The TEM-BF images showed that the Pd NPs remained monodispersed and that particle size did not change dramatically compared to that of the preannealed sample. Moreover, thermal decompositions of Pd@MOF-1, Pd@MOF-2(Cd), or Pd@MOF-3 were compared with that of bare MOFs by the TGA method up to 800 °C to confirm their thermal stability (Supporting Information). The stability of the MOFs remained intact even after loading of the Pd NPs. Interestingly, the weight differences between MOFs and Pd@MOFs after decomposition also gave an indication about the amount of Pd loaded into MOFs. Therefore, the current results suggest that Pd@MOFs are excellent catalysts for high temperature catalytic reactions.

CONCLUSIONS

In conclusion, for the purpose of heterogeneous catalysis, three ethynyl functionalized MOFs with variable pore size have been used for the stabilization of Pd NPs. Pore sizes of the MOFs were controlled by tuning the length of the dipyriddy pillar. The interior ethynyl moieties are strategically utilized for loading of the large amount of Pd NPs through its distinct π -donation and π -acceptor characteristics of the ethynyl groups. The Pd loading amount in the present cases is dependent on the porosity of the MOFs. However, in contrast to the earlier reports where NPs are generally agglomerated when attempting to increase loading amount, these ethynyl functionalized MOFs were able to load a significantly large amount of Pd NPs (~27 wt %) without altering monodispersity and particle size. The preparation of NPs involved two distinct steps: adsorption of metal ions inside MOFs pores followed by the reduction of metal ions. In this contribution, we have also demonstrated that the size of the NPs can be tuned depending upon the porosity of the chosen MOFs. Finally, the Pd@MOFs were used for heterogeneous

Heck-coupling and hydrogenation reactions using several aromatic iodides/bromides and alkenes, respectively. Both types of reactions were very efficient even in the presence of an extremely small amount of catalyst. Most importantly, it has been shown that under a particular reaction condition selective coupling of aryl iodides and alkene takes place in the presence of bromide. Under another condition, both iodide and bromide undergo coupling reactions with alkene. Moreover, these Pd@MOFs were recycled several times with excellent catalytic activities. Importantly, these catalysts are also stable at higher temperature with respect to NP agglomeration and can be used for the other high temperature catalytic reactions.

ASSOCIATED CONTENT

Supporting Information

The Supporting Information is available free of charge on the ACS Publications website at DOI: 10.1021/acs.inorgchem.5b02739.

Crystallographic data, additional PXRD, TEM images XPS, gas adsorption studies, and characterizations of catalytic products (PDF)
X-ray data (CIF)

AUTHOR INFORMATION

Corresponding Author

*Tel: +91-80-2293-3352. Fax: +91-80-2360-1552. E-mail: psm@ipc.iisc.ernet.in.

Notes

The authors declare no competing financial interest.

ACKNOWLEDGMENTS

We are grateful to the Department of Science and Technology (DST), India for financial support. We are thankful to Professor B. R. Jagirdar and Mr. Sourav Ghosh for providing the facilities to conduct the hydrogenation reaction.

REFERENCES

- (1) Somorjai, G. A.; Li, Y. *Introduction to Surface Chemistry and Catalysis*; 2nd ed.; Wiley-VCH: New York, 2010.
- (2) (a) Burda, C.; Chen, X.; Narayanan, R.; El-Sayed, M. A. *Chem. Rev.* **2005**, *105*, 1025–1102. (b) Mostafa, S.; Behafarid, F.; Croy, J. R.; Ono, L. K.; Li, L.; Yang, J. C.; Frenkel, A. I.; Cuenya, B. R. *J. Am. Chem. Soc.* **2010**, *132*, 15714–15719. (c) Xiong, Y.; Wiley, B. J.; Xia, Y. *Angew. Chem., Int. Ed.* **2007**, *46*, 7157–7159.
- (3) *Nanoscale Materials in Chemistry*; 2nd ed.; Wiley-VCH: New York, 2009.
- (4) Schlögl, R.; Abd, H.; Sharifah, B. *Angew. Chem., Int. Ed.* **2004**, *43*, 1628–1637.
- (5) White, R. J.; Luque, R.; Budarin, V. L.; Clark, J. H.; Macquarrie, D. J. *Chem. Soc. Rev.* **2009**, *38*, 481–494.
- (6) (a) Farha, O. K.; Özgür Yazaydin, A.; Eryazici, I.; Malliakas, C. D.; Hauser, B. G.; Kanatzidis, M. G.; Nguyen, S. T.; Snurr, R. Q.; Hupp, J. T. *Nat. Chem.* **2010**, *2*, 944–948. (b) Ferey, G. *Chem. Soc. Rev.* **2008**, *37*, 191–214. (c) Kitagawa, S.; Kitaura, R.; Noro, S.-i. *Angew. Chem., Int. Ed.* **2004**, *43*, 2334–2375. (d) Lee, J.; Farha, O. K.; Roberts, J.; Scheidt, K. A.; Nguyen, S. T.; Hupp, J. T. *Chem. Soc. Rev.* **2009**, *38*, 1450–1459. (e) Li, H.; Eddaoudi, M.; O’Keeffe, M.; Yaghi, O. M. *Nature* **1999**, *402*, 276–279. (f) Li, J.-R.; Sculley, J.; Zhou, H.-C. *Chem. Rev.* **2012**, *112*, 869–932. (g) Long, J. R.; Yaghi, O. M. *Chem. Soc. Rev.* **2009**, *38*, 1213–1214. (h) O’Keeffe, M. *Chem. Soc. Rev.* **2009**, *38*, 1215–1217. (i) Stock, N.; Biswas, S. *Chem. Rev.* **2012**, *112*, 933–969. (j) Yaghi, O. M.; Li, H. *J. Am. Chem. Soc.* **1995**, *117*, 10401–10402.

- (7) (a) Aijaz, A.; Xu, Q. *J. Phys. Chem. Lett.* **2014**, *5*, 1400–1411. (b) Dhakshinamoorthy, A.; Garcia, H. *Chem. Soc. Rev.* **2012**, *41*, 5262–5284. (c) Meilikhov, M.; Yusenko, K.; Esken, D.; Turner, S.; Van Tendeloo, G.; Fischer, R. A. *Eur. J. Inorg. Chem.* **2010**, *2010*, 3701–3714. (d) Rosler, C.; Fischer, R. A. *CrystEngComm* **2015**, *17*, 199–217.
- (8) (a) Esken, D.; Turner, S.; Lebedev, O. I.; Van Tendeloo, G.; Fischer, R. A. *Chem. Mater.* **2010**, *22*, 6393–6401. (b) Hermes, S.; Schröter, M.-K.; Schmid, R.; Rhodeir, L.; Muhler, M.; Tissler, A.; Fischer, R. W.; Fischer, R. A. *Angew. Chem., Int. Ed.* **2005**, *44*, 6237–6241. (c) Ishida, T.; Nagaoka, M.; Akita, T.; Haruta, M. *Chem. - Eur. J.* **2008**, *14*, 8456–8460. (d) Jiang, H.-L.; Lin, Q.-P.; Akita, T.; Liu, B.; Ohashi, H.; Oji, H.; Honma, T.; Takei, T.; Haruta, M.; Xu, Q. *Chem. - Eur. J.* **2011**, *17*, 78–81. (e) Jiang, H.-L.; Liu, B.; Akita, T.; Haruta, M.; Sakurai, H.; Xu, Q. *J. Am. Chem. Soc.* **2009**, *131*, 11302–11303. (f) Schröder, F.; Esken, D.; Cokoja, M.; van den Berg, M. W. E.; Lebedev, O. I.; Van Tendeloo, G.; Walaszek, B.; Buntkowsky, G.; Limbach, H.-H.; Chaudret, B.; Fischer, R. A. *J. Am. Chem. Soc.* **2008**, *130*, 6119–6130. (g) Liu, X.-H.; Ma, J.-G.; Niu, Z.; Yang, G.-M.; Cheng, P. *Angew. Chem., Int. Ed.* **2015**, *54*, 988–991.
- (9) (a) Park, Y. K.; Choi, S. B.; Nam, H. J.; Jung, D.-Y.; Ahn, H. C.; Choi, K.; Furukawa, H.; Kim, J. *Chem. Commun.* **2010**, *46*, 3086–3088. (b) Proch, S.; Herrmannsdörfer, J.; Kempe, R.; Kern, C.; Jess, A.; Seyfarth, L.; Senker, J. *Chem. - Eur. J.* **2008**, *14*, 8204–8212.
- (10) (a) Henschel, A.; Gedrich, K.; Kraehnert, R.; Kaskel, S. *Chem. Commun.* **2008**, 4192–4194. (b) Hwang, Y. K.; Hong, D.-Y.; Chang, J.-S.; Jhung, S. H.; Seo, Y.-K.; Kim, J.; Vimont, A.; Daturi, M.; Serre, C.; Férey, G. *Angew. Chem., Int. Ed.* **2008**, *47*, 4144–4148. (c) Jiang, H.-L.; Akita, T.; Ishida, T.; Haruta, M.; Xu, Q. *J. Am. Chem. Soc.* **2011**, *133*, 1304–1306. (d) Li, H.; Zhu, Z.; Zhang, F.; Xie, S.; Li, H.; Li, P.; Zhou, X. *ACS Catal.* **2011**, *1*, 1604–1612. (e) Park, T.-H.; Hickman, A. J.; Koh, K.; Martin, S.; Wong-Foy, A. G.; Sanford, M. S.; Matzger, A. J. *J. Am. Chem. Soc.* **2011**, *133*, 20138–20141. (f) Wang, C.; deKrafft, K. E.; Lin, W. J. *J. Am. Chem. Soc.* **2012**, *134*, 7211–7214. (g) Zlotea, C.; Campesi, R.; Cuevas, F.; Leroy, E.; Dibandjo, P.; Volklinger, C.; Loiseau, T.; Férey, G.; Latroche, M. *J. Am. Chem. Soc.* **2010**, *132*, 2991–2997.
- (11) Lu, G.; Li, S.; Guo, Z.; Farha, O. K.; Hauser, B. G.; Qi, X.; Wang, Y.; Wang, X.; Han, S.; Liu, X.; DuChene, J. S.; Zhang, H.; Zhang, Q.; Chen, X.; Ma, J.; Loo, S. C. J.; Wei, W. D.; Yang, Y.; Hupp, J. T.; Huo, F. *Nat. Chem.* **2012**, *4*, 310–316.
- (12) Aijaz, A.; Karkamkar, A.; Choi, Y. J.; Tsumori, N.; Rönnebro, E.; Autrey, T.; Shioyama, H.; Xu, Q. *J. Am. Chem. Soc.* **2012**, *134*, 13926–13929.
- (13) (a) Hartley, F. R. *Chem. Rev.* **1969**, *69*, 799–844. (b) Zhang, K.; Cutler, J. I.; Zhang, J.; Zheng, D.; Auyeung, E.; Mirkin, C. A. *J. Am. Chem. Soc.* **2010**, *132*, 15151–15153. (c) Zhang, S.; Chandra, K. L.; Gorman, C. B. *J. Am. Chem. Soc.* **2007**, *129*, 4876–4877.
- (14) Gole, B.; Sanyal, U.; Mukherjee, P. S. *Chem. Commun.* **2015**, *51*, 4872–4875.
- (15) (a) Kreno, L. E.; Leong, K.; Farha, O. K.; Allendorf, M.; Van Duyne, R. P.; Hupp, J. T. *Chem. Rev.* **2012**, *112*, 1105–1125. (b) Wu, H.; Gong, Q.; Olson, D. H.; Li, J. *Chem. Rev.* **2012**, *112*, 836–868.
- (16) Kampers, F. W. H.; Engelen, C. W. R.; Van Hooff, J. H. C.; Koningsberger, D. C. *J. Phys. Chem.* **1990**, *94*, 8574–8578.
- (17) Gole, B.; Bar, A. K.; Mukherjee, P. S. *Chem. - Eur. J.* **2014**, *20*, 2276–2291.
- (18) (a) Amatore, C.; Jutand, A. *Acc. Chem. Res.* **2000**, *33*, 314–321. (b) Kim, S.-W.; Kim, M.; Lee, W. Y.; Hyeon, T. *J. Am. Chem. Soc.* **2002**, *124*, 7642–7643. (c) Miyaura, N.; Suzuki, A. *Chem. Rev.* **1995**, *95*, 2457–2483. (d) Moreno-Mañas, M.; Pleixats, R. *Acc. Chem. Res.* **2003**, *36*, 638–643. (e) Wu, X.-F.; Anbarasan, P.; Neumann, H.; Beller, M. *Angew. Chem., Int. Ed.* **2010**, *49*, 9047–9050.
- (19) (a) Huang, J.; Jiang, T.; Gao, H.; Han, B.; Liu, Z.; Wu, W.; Chang, Y.; Zhao, G. *Angew. Chem.* **2004**, *116*, 1421–1423. (b) Jiang, Y.; Gao, Q. *J. Am. Chem. Soc.* **2006**, *128*, 716–717. (c) Kwon, M. S.; Kim, N.; Park, C. M.; Lee, J. S.; Kang, K. Y.; Park, J. *Org. Lett.* **2005**, *7*, 1077–1079. (d) Niu, Y.; Yeung, L. K.; Crooks, R. M. *J. Am. Chem. Soc.* **2001**, *123*, 6840–6846. (e) Yamada, Y. M. A.; Yuyama, Y.; Sato, T.; Fujikawa, S.; Uozumi, Y. *Angew. Chem., Int. Ed.* **2014**, *53*, 127–131.
- (20) Joo, S. H.; Park, J. Y.; Tsung, C.-K.; Yamada, Y.; Yang, P.; Somorjai, G. A. *Nat. Mater.* **2009**, *8*, 126–131.